Research Article | Vol. 26, No. 5 | 5 Mar 2018 | OPTICS EXPRESS 5300
Optics EXPRESS

Escape from an optoelectronic tweezer trap: experimental results and simulations

SHUAILONG ZHANG,[1,2,3,9] ADELE NIKITINA,[3] YUJIE CHEN,[4] YANFENG ZHANG,[4] LIN LIU,[4] ANDREW G. FLOOD,[5] JOAN JUVERT,[6] M. DEAN CHAMBERLAIN,[1,2,3] NAZIR P. KHERANI,[5,7] STEVEN L. NEALE,[8,10] AND AARON R. WHEELER,[1,2,3,*]

[1]*Donnelly Centre for Cellular and Biomolecular Research, 160 College Street, Toronto, M5S 3E1, Canada*
[2]*Department of Chemistry, University of Toronto, 80 St George Street, Toronto, M5S 3H6, Canada*
[3]*Institute of Biomaterials and Biomedical Engineering, 164 College Street, Toronto, M5S 3G9, Canada*
[4]*State Key Laboratory of Optoelectronic Materials and Technologies, School of Electronics and Information Technology, Sun Yat-sen University, Guangzhou, 510275, China*
[5]*Department of Electrical and Computer Engineering, University of Toronto, 10 King's College Road, Toronto, M5S 3G4, Canada*
[6]*Photonics Research Group, INTEC-Department, Ghent University-IMEC, Technologiepark-Zwijnaarde 15 iGent, 9052 Gent, Belgium*
[7]*Department of Materials Science and Engineering, University of Toronto, 184 College Street, Toronto, M5S 3E4, Canada*
[8]*School of Engineering, University of Glasgow, Glasgow, Scotland, G12 8LT, UK*
[9]*shuailong.zhang@utoronto.ca*
[10]*steven.neale@glasgow.ac.uk*
[*] *aaron.wheeler@utoronto.ca*

Abstract: Optoelectronic tweezers (OET) are a microsystem actuation technology capable of moving microparticles at mm s^{-1} velocities with nN forces. In this work, we analyze the behavior of particles manipulated by negative dielectrophoresis (DEP) forces in an OET trap. A user-friendly computer interface was developed to generate a circular rotating light pattern to control the movement of the particles, allowing their force profiles to be conveniently measured. Three-dimensional simulations were carried out to clarify the experimental results, and the DEP forces acting on the particles were simulated by integrating the Maxwell stress tensor. The simulations matched the experimental results and enabled the determination of a new "hopping" mechanism for particle-escape from the trap. As indicated by the simulations, there exists a vertical DEP force at the edge of the light pattern that pushes up particles to a region with a smaller horizontal DEP force. We propose that this phenomenon will be important to consider for the design of OET micromanipulation experiments for a wide range of applications.

OCIS codes: (350.4855) Optical tweezers or optical manipulation; (120.4880) Optomechanics; (120.4640) Optical instruments.

References and links

1. P. Y. Chiou, A. T. Ohta, and M. C. Wu, "Massively parallel manipulation of single cells and microparticles using optical images," Nature **436**(7049), 370–372 (2005).
2. A. Jamshidi, S. L. Neale, K. Yu, P. J. Pauzauskie, P. J. Schuck, J. K. Valley, H. Y. Hsu, A. T. Ohta, and M. C. Wu, "Nanopen: Dynamic, Low-power, and Light-actuated Patterning of Nanoparticles," Nano Lett. **9**(8), 2921–2925 (2009).
3. H. Hwang and J. K. Park, "Optoelectrofluidic platforms for chemistry and biology," Lab Chip **11**(1), 33–47 (2011).
4. S. Xie, X. Wang, N. Jiao, S. Tung, and L. Liu, "Programmable micrometer-sized motor array based on live cells," Lab Chip **17**(12), 2046–2053 (2017).
5. A. T. Ohta, P. Y. Chiou, T. H. Han, J. C. Liao, U. Bhardwaj, E. R. B. McCabe, F. Yu, R. Sun, and M. C. Wu, "Dynamic cell and microparticle control via optoelectronic tweezers," J. Microelectromech. Syst. **16**(3), 491–499 (2007).
6. M. Woerdemann, C. Alpmann, M. Esseling, and C. Denz, "Advanced optical trapping by complex beam shaping," Laser Photon. Rev. **7**(6), 839–854 (2013).

#309982 https://doi.org/10.1364/OE.26.005317
Journal © 2018 Received 30 Oct 2017; revised 4 Jan 2018; accepted 5 Jan 2018; published 21 Feb 2018

Optics EXPRESS

7. S. L. Neale, M. Mazilu, J. I. B. Wilson, K. Dholakia, and T. F. Krauss, "The resolution of optical traps created by light induced dielectrophoresis (LIDEP)," Opt. Exp. **15**(20), 12619–12626 (2007).
8. A. Jamshidi, P. J. Pauzauskie, P. J. Schuck, A. T. Ohta, P. Y. Chiou, J. Chou, P. Yang, and M. C. Wu, "Dynamic manipulation and separation of individual semiconducting and metallic nanowires," Nat. Photon. **2**(2), 86–89 (2008).
9. P. J. Pauzauskie, A. Jamshidi, J. K. Valley, J. H. Satcher Jr, and M. C. Wu, "Parallel trapping of multiwalled carbon nanotubes with optoelectronic tweezers," Appl. Phys. Lett. **95**(11), 113104 (2009).
10. S. M. Yang, T. M. Yu, H. P. Huang, M. Y. Ku, L. Hsu, and C. H. Liu, "Dynamic manipulation and patterning of microparticles and cells by using TiOPc-based optoelectronic dielectrophoresis," Opt. Lett. **35**(12), 1959–1961 (2010).
11. S. L. Neale, A. T. Ohta, H. Y. Hsu, J. K. Valley, A. Jamshidi, and M. C. Wu, "Trap profiles of projector based optoelectronic tweezers (OET) with HeLa cells," Opt. Exp. **17**(7), 5231–5239 (2009).
12. A. T. Ohta, M. Garcia, J. K. Valley, L. Banie, H.-Y. Hsu, A. Jamshidi, S. L. Neale, T. Lue, and M. C. Wu, "Motile and non-motile sperm diagnostic manipulation using optoelectronic tweezers," Lab Chip **10**(23), 3213–3217 (2010).
13. G. B. Lee, C. J. Chang, C. H. Wang, M. Y. Lu, and Y. Y. Luo, "Continuous medium exchange and optically induced electroporation of cells in an integrated microfluidic system," Microsyst. Nanoeng. **1**, 15007 (2015).
14. S. Zhang, Y. Liu, J. Juvert, P. Tian, J. C. Navarro, J. M. Cooper, and S. L. Neale, "Use of optoelectronic tweezers in manufacturing - accurate solder bead positioning," Appl. Phys. Lett. **109**(22), 221110 (2016).
15. Y. Yang, Y. Mao, K. S. Shin, C. O. Chui, and P. Y. Chiou, "Self-Locking Optoelectronic Tweezers for Single-Cell and Microparticle Manipulation across a Large Area in High Conductivity Media," Sci. Rep. **6**, 22630 (2016).
16. J. Juvert, S. Zhang, I. Eddie, C. J. Mitchell, G. T. Reed, J. S. Wilkinson, A. Kelly, and S. L. Neale, "Micromanipulation of InP lasers with optoelectronic tweezers for integration on a photonic platform," Opt. Exp. **24**(16), 18163–18175 (2016).
17. S. Zhang, J. Juvert, J. M. Cooper, and S. L. Neale, "Manipulating and assembling metallic beads with optoelectronic tweezers," Sci. Rep. **6**, 32840 (2016).
18. S. Zhang, Y. Liu, Y. Qian, W. Li, J. Juvert, P. Tian, J. Navarro, A. W. Clark, E. Gu, M. D. Dawson, J. M. Cooper, and S. L. Neale, "Manufacturing with light - micro-assembly ofcopto-electronic microstructures," Opt. Exp. **25**(23), 28838–28850 (2017).
19. S. Zhang, A. Nikitina, Y. Chen, Y. Zhang, L. Liu, A. G. Flood, J. Juvert, D. Chamberlain, N. P. Kherani, S. L. Neale, and A. R. Wheeler, "Carthwheel," figshare (2017) [retrieved 24 Oct 2017], https://doi.org/10.6084/m9.figshare.5536627.
20. S. B. Huang, M. H. Wu, Y. H. Lin, C. H. Hsieh, C. L. Yang, H. C. Lin, C. P. Tseng, and G. B. Lee, "High-purity and labelfree isolation of circulating tumor cells (CTCs) in a microfluidic platform by using optically-induced-dielectrophoretic (ODEP) force," Lab Chip **13**(7), 1371–1383 (2013).
21. A. Zarowna-Dabrowska, S. L. Neale, D. Massoubre, J. McKendry, B. R. Rae, R. K. Henderson, M. J. Rose, H. Yin, J. M. Cooper, E. Gu, and M. M. Dawson, "Miniaturized optoelectronic tweezers controlled by GaN micro-pixel light emitting diode arrays," Opt. Exp. **19**(3), 2720–2728 (2011).
22. R. Pethig, "Dielectrophoresis: Status of the theory, technology, and applications," Biomicrofluidics **4**(2), 022811 (2010).
23. X. Wang, X. B. Wang, and P. R. C. Gascoyne, "General expressions for dielectrophoretic force and electrorotational torque derived using the Maxwell stress tensor method," J. Electrostat. **39**(4), 277–295 (1997).
24. S. Kumar and P. J. Hesketh, "Interpretation of ac dielectrophoretic behavior of tin oxide nanobelts using Maxwell stress tensor approach modeling," Sensor Actuat. B Chem. **161**(1), 1198–1208 (2012).
25. K. H. Kang, I. S. Kang, and C. M. Lee, "Wetting tension due to Coulombic interaction in charge-related wetting phenomena," Langmuir **19**(13), 5407–5412 (2003).
26. M. Abdelgawad, P. Park, and A. R. Wheeler, "Optimization of device geometry in single-plate digital microfluidics," J. Appl. Phys. **105**(9), 094506 (2009).

1. Introduction

Optoelectronic tweezers (OET) is an opto-electro-fluidic micromanipulation technology that uses light-induced dielectrophoresis (DEP) for touch-free actuation of micro-scale objects in physical, chemical and biomedical studies [1–5]. Compared to conventional optical tweezers, OET traps exert a much stronger manipulation force for a given intensity of light, and in addition OET is well suited for massively parallel manipulation [1, 6, 7]. To date, there has been demonstration of OET manipulation of many nano- and micro-scale objects, ranging from semiconductor nanowires and carbon nanotubes [8, 9], to cells and particles on the order of tens of microns [10–15], to photonic/electronic devices with sizes greater than 100 microns [16, 17].

OET has been reported to manipulate micro particles at velocities of several mm s^{-1} propelled by forces of up to nano-Newton levels [14, 17, 18]. This suggests utility for OET as a micro-assembly tool, making it important to characterize its effectiveness to manipulate targeted objects in terms of the highest achievable positioning speed and accuracy. These properties are typically

Optics EXPRESS

determined by measuring the viscous drag force imposed on a trapped object that causes it to escape the OET trap. However, there has been a lack of relevant studies concerning the mechanism of an object's escape from an OET trap, a topic that will be important for users who wish to use OET for efficient manipulation of micro-objects in various conditions.

In this work, we introduce a new method to evaluate the behavior of particles trapped in OET traps and used this technique to study their mechanism of escape. A user-friendly computer interface was developed to allow convenient control of a rotating light pattern. Particles experiencing negative DEP (bounded on all sides by the edge of a moving light pattern) were made to move in a circular path on a microscope stage, such that the particles' velocities and trajectories could be observed under different conditions. At high velocities, particles were observed to escape the trap vertically (into the suspending medium) before settling back onto the surface. Three-dimensional (3D) numerical simulations of electrical field distribution indicated that the vertical displacement phenomenon occurs when the particle experiences the strongest DEP force (at the boundary of the light pattern), lifting the trapped particle to a region where viscous drag exceeds the local horizontal DEP force, thereby forcing it to escape OET confinement. We believe this is the first study to consider the vertical DEP force and its influence on the behavior of particles in an OET system. We propose that the escape mechanism clarified in this work is likely to be a general one for objects manipulated by negative DEP in an OET trap, which will be important to consider in the future design of OET-enabled micro-assembly tools for a wide range of applications [1–5].

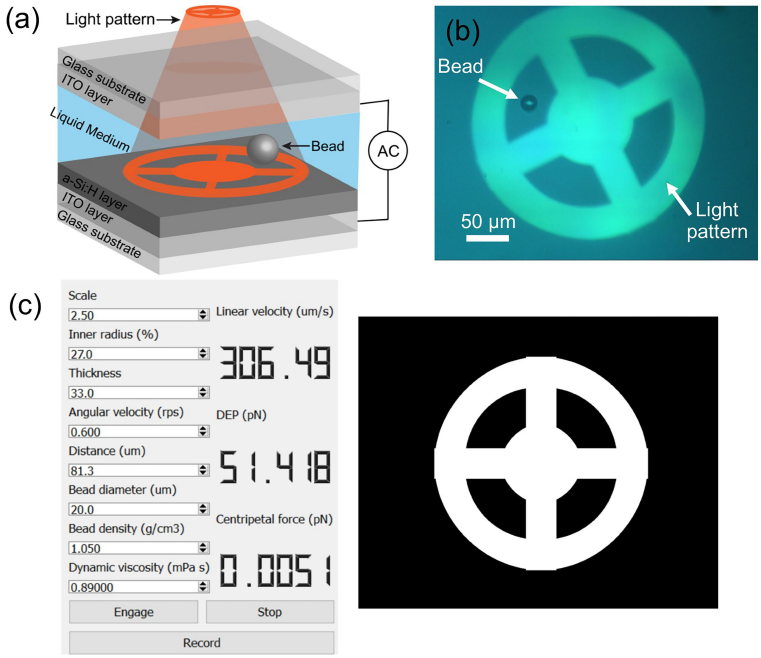

Fig. 1. Optoelectronic tweezers (OET) system used to evaluate object-escape behavior. (a) 3D schematic diagram of the OET device (not to scale). (b) Microscope image of a 20-μm-diameter polystyrene bead manipulated by the cartwheel-shaped light pattern. See Visualization 1 for a video showing the movement of the bead. (c) Reproduction of graphical user-interface from the custom control software used to control the experiments and collect data. The source code of the software is provided in Code 1 (Ref. [19]).

Optics EXPRESS

2. Methods

Unless otherwise specified, reagents were purchased from Sigma Chemical (Oakville, ON, Canada) or Fisher Scientific Canada (Ottawa, ON, Canada). Figure 1(a) shows a 3D schematic diagram of the OET device used in this work, which comprises two planar electrodes separated by a spacer. The electrodes were formed from two glass slides each coated on one side with a 200-nm-thick layer of indium tin oxide (ITO) (Riley Supplies, Canada). The bottom electrode was coated with an additional layer of 1-μm-thick hydrogenated amorphous silicon (a-si:H) atop the ITO, applied via rf plasma enhanced chemical vapor deposition. A 150-μm-thick spacer formed a thin chamber between the two electrodes, within which beads were manipulated. Spherical polystyrene beads (Polysciences, Inc., USA), in most cases with 20 μm diameter but in some cases with 4.5, 7, 10 or 45 μm diameter, were suspended in deionized water containing Tween 20 (0.05% v/v); the conductivity of the solution was measured to be 5.0 mS/m. In a typical experiment, an aliquot of bead-suspension (40 μL) was pipetted into the chamber of the OET device, which was then driven by an AC potential (sine wave, in most cases 20 V_{pp}, 50 kHz) produced by a function generator (0.5-3 V_{pp}) (33220A, Agilent, USA) connected to an amplifier (10×, 50 Ω output) (WA301, Thurlby Thandar Instruments, UK). The optical setup was similar to that used in previous work [16–18]: a light pattern from a projector (1650, Dell, USA) bearing a digital micromirror display was focused by a plano-convex lens (LA1301-A-N-BK7, Thorlabs, USA) into an upright microscope (DM 2000, Leica, USA) (10× objective) and projected on the surface of the photoconductive layer (a-Si:H) from the top side of the OET device. More details of the optical setup can be found in our previous work [16–18].

A custom computer program was developed to project and control the position of a cartwheel-shaped light pattern. As shown in Fig. 1(b), the illumination pattern comprises a filled circle (inner) concentric with a hollow circle (outer) bisected with a cross to generate four non-illuminated "pockets". In a typical experiment, the pattern was programmed to rotate at various velocities, such that beads trapped in the pockets were made to move with the pattern. A video illustrating the manipulation of a 20-μm-diameter bead at various rotational speeds can be found in Visualization 1. Shown in Fig. 1(c) is a graphical user interface, which was developed to allow the user to set input parameters (e.g., scale, inner radius, thickness). For the data reported here, the cartwheel pattern's central circle diameter and outer circle inner-diameter were set to 100 μm and 200 μm, respectively, and the line segment width was set to 40 μm. To make the program available to other users, the source code is provided in supplementary Code 1 (Ref. [19]).

Beads moving in the OET trap were observed using a high-definition camera with a frame rate of 60 fps (BioVID HD 1080+, LW Scientific, USA). In each experiment, a selected velocity was established, after which a 20-second video was collected to record the bead's behavior. Subsequently, ToupView image analysis software (LW Scientific, USA) was used to extract five frames at random from the video and to measure the displacement D between the bead and the light pattern. The five measurements of D were averaged and recorded for each velocity evaluated.

Numerical simulations were carried out in COMSOL Multiphysics using the AC/DC module (COMSOL Inc., Burlington, MA, accessed via license obtained through CMC Microsystems, Kingston, Canada). The AC/DC module uses the quasi-static approximation which assumes that the dimensions of the volume under investigation are small compared to the wavelength of the applied AC signal. This assumption is justified in this work as the volume modelled is bounded by 150 μm across the X plane, Y plane and Z plane, respectively, while the wavelength of the applied AC signal is 6×10^3 m. The boundary conditions of the model were set to perfect electrical insulation at the sides of the volume and a continuation boundary was set for all interior boundaries. The top boundary was set to 0 V and the bottom boundary set to 20 V to simulate the applied AC signal, which was set to 50 kHz. Conductivities σ and permittivities ε used in the model included $\sigma_{silicon,light} = 1\times10^{-4}$ S/m, $\sigma_{silicon,dark} = 1\times10^{-6}$ S/m, $\sigma_{medium} = 5\times10^{-3}$

Optics EXPRESS

S/m, $\varepsilon_{medium} = 80$, $\sigma_{bead} = 1 \times 10^{-14}$ S/m, and $\varepsilon_{medium} = 2.4$. Finally, the model employed a free tetrahedral mesh with a minimum element size of 0.227 μm, a maximum element size of 5.29 μm, an element growth rate of 1.35, a resolution of curvature of 0.3, and a resolution of narrow regions of 0.85.

3. Experimental results and discussion

OET traps used to manipulate particles often rely on negative DEP - that is, a "pocket" of light is projected to surround the particle, and the negative DEP forces cause the particle to remain in the pocket as the light pattern is moved [1, 4, 5, 11, 12]. Previous approaches to evaluating OET object-trapping force in such cases have involved moving either the OET trap or a microscope stage linearly [11, 14, 17] at different velocities. These systems are not ideal, as the large working area results in frequent experimental interruptions caused by collisions between the trapped bead and debris or other beads. To overcome this challenge, we developed a system in which a cartwheel-shaped light pattern (bearing four "pockets" or traps) is rotated at different frequencies, as shown in Fig. 1. The linear velocity of a bead trapped in this rotating system is easily determined from the angular velocity of the light pattern and the center-to-center distance between the bead and the light pattern can be observed in images collected with a camera. In this work, the Reynolds number for a 20-μm-diameter bead moving at a maximum linear velocity of 340 μm/s is 0.0082, suggesting that the system is in the laminar flow regime, verifying two experimental assumptions. First, the low inertial forces allow the estimation of DEP force responsible for bead motion to be equivalent to the viscous drag force, which is given by Stoke's law [7, 11, 14]:

$$F_{DEP} = F_{drag} \tag{1}$$

$$F_{drag} = 6\pi\eta r v \tag{2}$$

where η is the viscosity of the liquid, r is the radius of the bead and v is velocity of the bead. Since in these experiments gravity forces the bead to settle in proximity to the device surface, Faxen's correction based on the radius of the microsphere (10 μm) was used to adjust the calculation of viscous drag force and DEP force [7, 14, 17, 20]. Second, the low inertial forces justify the use of a rotary particle movement path, noting that in a high Reynolds number environment, the particle would be continually accelerating against its inertia but the low Reynold's number system can be approximated as producing a continuous linear velocity.

To study the behavior of particles in the OET trap, the rotational speed of the cartwheel-shaped light pattern was gradually increased until the bead was observed to no longer be pushed forward by the light pattern, thus escaping from the trap. As shown in Figs. 2(a) and 2(b), the bead moves toward the edge of the light pattern as its velocity increases, indicating that there exists a stronger negative horizontal DEP force (pushing against the bead in the plane of the device surface) to maintain a larger velocity for the bead and keep it in the trap (see Visualization 1 for more details). Stated another way, the displacement D between the bead center and the center of the light pattern that pushes the bead decreases as the velocity increases. By measuring D at varying velocities, a force profile can be plotted of horizontal DEP force experienced by the bead (from Eq. 1 and Eq. 2, applying a Faxen's correction ratio of 3.1) at different positions in the trap. Figure 2(c) shows the measured force profile for beads manipulated in the trap at different velocities.

A numerical simulation was developed to assist in understanding the observed bead behavior. Previous models of beads manipulated by OET traps have been two-dimensional [11, 14, 16, 17, 21]; here, a 3D model was used in an attempt to achieve a closer match to experimental observations. The model was applied to evaluate two cases - an OET light pattern with a trapped bead, and an OET light pattern without. A schematic of the model with the bead is shown in Fig. 3(a), where the model length (X axis), width (Y axis), height (Z axis) are all set to 150 μm. The trap created by the light pattern is located at the central bottom of the model ranging from -20 to 20 μm in X

Optics EXPRESS

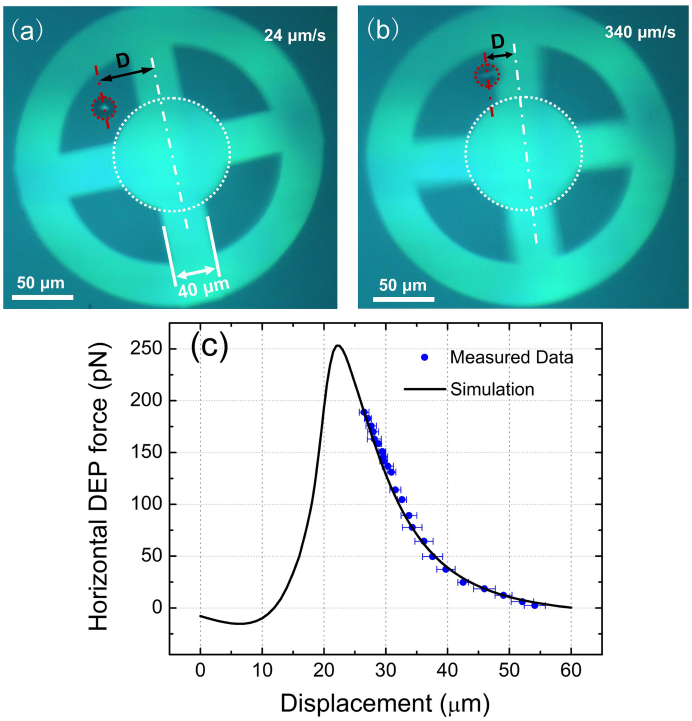

Fig. 2. OET-trap bead manipulation. Microscope images of a 20-μm-diameter polystyrene bead being moved at linear velocities of (a) 24 μm/s and (b) 340 μm/s in the cartwheel-shaped light pattern. In these images, the cartwheel is rotating counter-clockwise, the bead is outlined in a red dashed line, and displacement D indicates the distance between bead center and the center of the line that pushes it. See Visualization 1 for a video showing the detailed process. (c) Plot of negative horizontal DEP force (experimental - blue markers; simulation - black line) as a function of D for beads manipulated at different velocities. Error bars for the experimental measurements represent ±1 standard deviation from five measurements for each condition. The simulation is a plot of corrected horizontal DEP force predicted by integrating the Maxwell Stress tensor for the system (described below).

direction and from -75 to 75 μm in Y direction. A 20-μm-diameter polystyrene bead is located at the right of the light pattern, straddling its edge. Figures 3(b) and 3(c) show the simulated electric potential distribution and the electric field distribution, respectively for this case. A schematic of the model without the bead is shown in Fig. 3(d), and Figs. 3(e) and 3(f) show the simulated electric potential distribution and the electric field distributions. As shown in Figs. 3(b) and 3(e), there is a large electric potential variation along Z-axis (from the liquid medium to the a-Si:H surface) in the central region relative to that found at the edges of the model, caused by the difference in conductivity between the illuminated and dark a-Si:H. While the trend is similar for both cases, note that the magnitude and distribution of electric potential in the medium are different with and without the bead. More importantly, the electric field distributions with (see Fig. 3(c)) and without (see Fig. 3(f)) the bead are dramatically different. The presence of the dielectric bead has a significant influence on the intensity and distribution of the surrounding electric field, differing from the case with no bead: note the difference in scales of the two heat-maps, with maximum/red at 10^6 V/m in panel (c) and maximum/red at 10^5 V/m in panel (f). These differences are caused by the differences in permittivity and conductivity of the dielectric material and the solution.

Optics EXPRESS

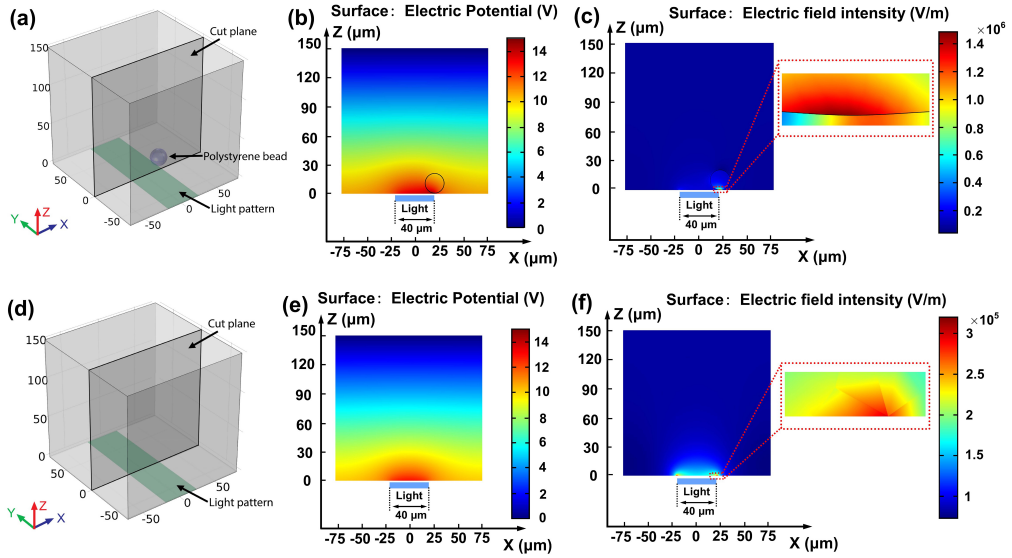

Fig. 3. 3D numerical simulations of the OET trap. (a,d) Schematics and plots of simulated electric potential (b,e) and electric field (c,f) for an OET trap formed by illuminating a 40-μm-wide light pattern (shaded in green) with (a-c) or without (d-f) a 20-μm-diameter polystyrene bead straddling the edge of the light pattern. Z-X cut planes in (a,d) form the basis for the plots in (b-f), in which the simulated electric potential and field are indicated in heat maps (blue = low, red - high). In (b,c), the bead is illustrated as an open black circle. In (c,f), the insets are a magnified portion of the 1 μm × 3 μm (Z × X) region encompassing the edge of the light pattern.

With the simulations of electric potential and field, we turned our attention to simulating the behavior of DEP force acting on the bead. DEP force is typically calculated using a classic dipole approximation method [22] in which the force acting on a spherical particle is expressed as:

$$F_{DEP} = 2\pi r^3 \varepsilon_m Re\left[K(\omega)\right] \nabla E^2 \tag{3}$$

where r is the radius of the particle, ε_m is the permittivity of the medium, $Re\left[K(\omega)\right]$ is the real component of the Clausius-Mossotti (CM) factor (which is dependent on angular frequency ω), and ∇E^2 is the gradient of the external electric field's square. This dipole approximation method is useful for qualitatively indicating whether positive or negative DEP is expected for particular material and fluid combinations, and in predicting the DEP trends for simple geometric arrangements. However, this approximation is strictly applicable only when the particle is much smaller than the scale of the field non-uniformity (and thus has little influence on the non-uniformity of the surrounding electric field [22]). As shown in Figs. 3(c) and 3(f), that criterion does not apply to the system described here.

With the limitations of Eq. 3 in mind, a second model of DEP force based on the integration of Maxwell stress tensor was used here. This method, which has been used previously to calculate DEP forces [16, 23, 24] as well as forces acting on droplets in digital microfluidics [25, 26], is derived from the Lorentz force law and can be expressed as:

$$\sigma_{ij} = \varepsilon_0 E_i E_j + \frac{1}{\mu_0} B_i B_j - \frac{1}{2}\left(\varepsilon_0 E^2 + \frac{1}{\mu_0} B^2\right)\delta_{ij} \tag{4}$$

where σ_{ij} is the ij element of the second rank Maxwell stress tensor, ε_0 is the vacuum permittivity, μ_0 is the vacuum permeability, E and B are the electric and magnetic fields, respectively, and δ_{ij}

Optics EXPRESS

is Kronecker's delta. The element σ_{ij} of the Maxwell stress tensor has a unit of force per unit area, and the ij element of the tensor can also be interpreted as the force per unit area parallel to the th ith axis crossing a surface normal to the jth axis. The diagonal elements represent the pulling forces while the off-diagonal elements represent the shear stress [16, 23]. Therefore, the total force acting on a volume of dielectric inside an electromagnetic field can be calculated by integrating the Maxwell stress tensor of the electromagnetic field over the surface area of the volume,

$$F_{DEP} = \oint_s \sigma \cdot n dS \tag{5}$$

where S represents the surface enclosing the bead and n represents the unit vector.

Using Eq. 5, we simulated the negative horizontal DEP force acting on beads with different displacement D for the model in Fig. 3(a) (assuming a Z-dimension position of the bead of 100 nm above the a-Si:H surface). The simulated horizontal DEP forces were found to be stronger than the measured forces in this system, suggesting that the beads used in experiments may experience greater frictional forces than predicted (including interactions with the surface). Additionally, the simulation assumes that some electrical potential is lost on contact resistance and thus does not drop across the liquid layer; experimentally this assumption may not hold true. Nevertheless, after scaling the simulation result by a factor of 0.43, there is a good match between the simulated (solid line) and measured (blue markers) results in Fig. 2(c). Further, the simulated negative horizontal force profile has a peak at the edge of the light pattern, which matches the experimental result that the bead experiences a stronger horizontal DEP force at the edge of the light pattern. An interesting phenomenon was also observed from the simulation and experimental results: in experiments, the bead escapes the trap prior to experiencing the maximum horizontal DEP force. Based on the simulation, the bead should experience a maximum horizontal DEP force of roughly 253 pN, with a displacement of 22 μm. However, in experiments, beads were always observed to escape the trap at (or before) reaching a displacement of 26.5 μm (which, according to the simulation, represents a horizontal DEP force of 189 pN). Note that this behavior is quite different from a particle moving under positive DEP in an OET system, in which trapped particles always reach maximum displacement and DEP force before escaping the trap [14, 17]. Since the horizontal DEP force balances the viscous drag force and keeps the bead in the trap, our initial hypothesis was that beads would escape the trap when the DEP force reaches its maximum and can no longer increase to match the viscous drag force.

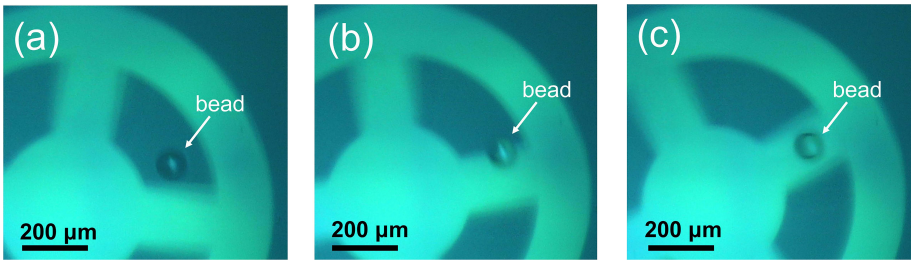

Fig. 4. Bead escape from an OET trap. (a)-(c) Video frames showing a 20-μm-diameter bead manipulated at a linear velocity of 489 μm/s, causing it to escape from the trap. See supplementary Visualization 2 for more details.

To understand the phenomenon of "premature" bead escape, the behavior of beads moved at high velocities was studied in greater detail. Figures 4(a)-4(c) comprises frames from a video of a 20-μm-diameter bead manipulated at a velocity such that it escapes from the trap (see Visualization 2 for more details). As shown, as the bead escapes from the trap, the image of the bead goes out of focus, indicating that it has moved vertically into the liquid medium. Returning

Optics EXPRESS

to the integrated Maxwell stress tensor simulations, we evaluated both vertical and horizontal DEP force - that is, negative DEP forces operating in both the X and Z dimensions. As expected from the data in Fig. 2, beads manipulated in the trap experience strong negative horizontal DEP forces (~10^2 pN, Fig. 5(a)). But beads manipulated in the trap also experience weaker negative vertical DEP forces (~10^1 pN, Fig. 5(b)); as far as we are aware, this is the first study to evaluate the effects of negative DEP forces acting in the vertical dimension over an OET trap. Note that the negative forces acting in both dimensions increase as the bead moves toward the edge of the light pattern (in the X dimension) and decrease as the bead moves upward (in the Z dimension).

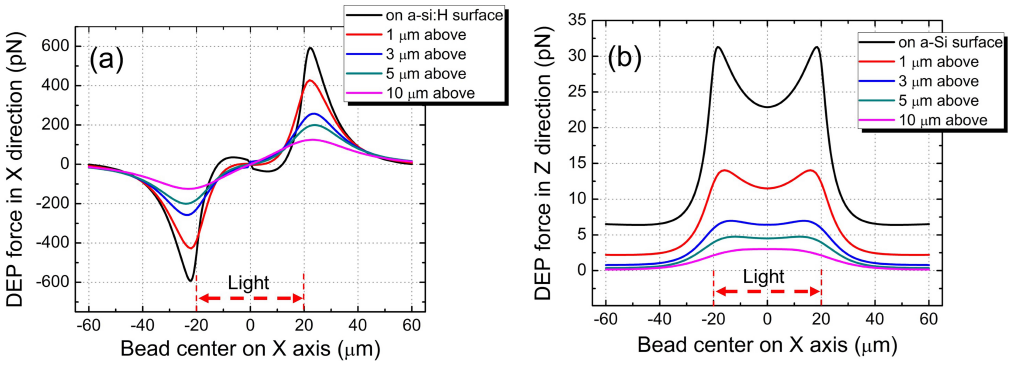

Fig. 5. Simulated DEP force profiles generated by the Maxwell Stress tensor method. (a) Simulated horizontal DEP force (in the X-dimension) and (b) simulated vertical DEP force (in the Z-dimension) for a 20-μm-diameter polystyrene bead as a function of bead position in the X-dimension (represented by the horizontal axes of the graphs) and Z-dimension (represented as different colored plots).

The simulations in Fig. 5 (as well as the observations in Fig. 4 and Visualization 2) suggest a mechanism for object escape from a negative DEP trap that has not been described previously. Specifically, as the trap velocity increases, the bead experiences a stronger horizontal viscous drag force and moves horizontally toward the edge of the light pattern, where it encounters a strong negative horizontal DEP force (see Fig. 5(a)). But as the bead approaches the edge of the light pattern, the negative vertical DEP force also increases (see Fig. 5(b)), and when this vertical DEP force exceeds the forces that keep the bead near the surface (i.e., gravity and electrostatic attraction to the surface), the bead begins to move upward into the liquid medium. As the bead moves upward, the horizontal DEP force decreases significantly, such that it no longer balances the horizontal viscous drag force. As a result, the bead begins to lag behind the rotational light pattern and subsequently escapes the light trap with a "hop".

Figure 6 is a schematic of the proposed bead "hopping" mechanism, driven primarily by the vertical DEP force experienced by the bead near the edge of the light pattern and the reduced horizontal DEP force experienced by the bead as it moves into the medium (above the surface). Note that the hopping mechanism is quite different from the case in which a trapped particle experiences positive DEP force in an OET system [14, 17], in which the positive vertical DEP force pulls the particle close to the surface. Therefore, for positive-DEP traps, the only competition is between the horizontal DEP force and the viscous drag force. We note that for the frequencies, conductivities, and permittivities that are commonly used in OET experiments, negative DEP forces are more commonly observed. Additionally, "hopping" behaviors were observed for particles under different device operating conditions and particles of various sizes. Visualization 3 shows the "hopping" behaviors of 20-μm-diameter polystyrene beads under 30 V at 25 kHz, 15 V at 30 kHz, 10 V at 50 kHz and 5 V at 10 kHz. Visualization 4 shows the "hopping" behaviors of polystyrene beads with diameters of 4.5, 7, 10 and 45 microns under the same bias of 20 V at

Optics EXPRESS

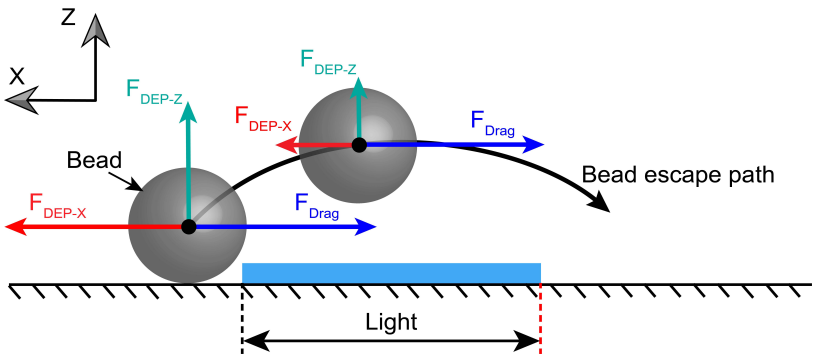

Fig. 6. Schematic of the proposed "hopping" mechanism for bead escape from a negative-DEP OET trap. When close to the surface, the negative horizontal DEP force (F_{DEP-X}, red arrow) compensates for viscous drag (F_{Drag}, blue arrow). But after being pushed into the Z-dimension by negative vertical DEP force (F_{DEP-Z}, green arrow), the negative horizontal force can no longer compensate for viscous drag, and the bead escapes from the trap. Note that the vertical and horizontal force-arrows are not to scale. See supplementary Visualization 3 for the "hopping" effect of beads under different device operating conditions and supplementary Visualization 4 for the "hopping" effect of beads with different sizes.

50 kHz. Thus, we propose that the hopping escape mechanism reported here is an important one for users to be aware of.

4. Conclusion

In this work, we report a new method to evaluate the behavior of objects manipulated by OET. A user-friendly computer interface was developed to generate a rotating cartwheel-shaped light pattern, enabling object position to be easily controlled and its DEP force profile to be conveniently measured. Systematic simulations in COMSOL Multiphysics suggested that the model object, a 20-μm-diameter polystyrene bead, significantly impacts the distribution of the surrounding electric field. This suggests that the widely used dipole approximation method for simulating DEP force is not appropriate; thus, the surface integral of the Maxwell stress tensor was used to simulate the DEP force acting on the bead, which estimated a similar trend in DEP-force profile relative to that found experimentally. The simulation and observations also highlighted the importance of considering both horizontal and vertical DEP forces in such systems. We observed and explain a new "hopping" escape-mechanism (driven by vertical DEP force) for objects trapped in a negative-DEP OET trap. Although polystyrene beads were mainly tested in this work, the general escape mechanism elucidated from this research is likely applicable to future use of OET-enabled micro-assembly tools for a wide range of applications.

Funding

Natural Sciences and Engineering Research Council of Canada (NSERC) (RGPIN 2014-06042, CREATE 482073-16); National Natural Science Foundation of China (NSFC) (51403244, 61323001, 11690031, 61490715, 11304401); Natural Science Foundation of Guangdong Province (2014A030313104); State Key Laboratory of Optoelectronic Materials and Technologies (OEMT), Sun Yat-sen University (SYSU) (Open Project: OEMT-2017-KF-03).